Signature dependence of $M1$ and $E2$ transition probabilities for the $i_{13/2}$ rotational band in ^{161}Dy

M. Oshima, E. Minehara, S. Ichikawa, and H. Iimura
Japan Atomic Energy Research Institute, Tokai-mura, Ibaraki 319-11, Japan

T. Inamura and A. Hashizume
The Institute of Physical and Chemical Research (RIKEN), Wako-shi, Saitama 351-01, Japan

H. Kusakari and S. Iwasaki
Chiba University, Yayoi-cho, Chiba 260, Japan

(Received 3 August 1987)

The ground-state rotational band of ^{161}Dy has been investigated through multiple Coulomb excitation with a beam of 250-MeV ^{58}Ni. γ-ray branchings and $E2/M1$ mixing ratios were determined up to the $\frac{25}{2}^+$ state by measurements of γ-ray angular distributions and γ-γ angular correlations. Nuclear lifetimes of levels up to $I=\frac{25}{2}$ have been measured using the Doppler-shift recoil-distance method. Considerable signature dependence was observed for $\Delta I=1$ $M1$ transition probabilities. $\Delta I=1$ $E2$ transition probabilities were found to decrease significantly as a function of spin. The results are compared with a microscopic model calculation based on the angular momentum projection method.

I. INTRODUCTION

It is well known that the Coriolis interaction acts most strongly on particles in high-spin orbitals. This interaction causes a strong perturbation to the rotational band based on the high-spin orbital. Recent data[1-4] on intraband transition probabilities for such high-spin rotational bands of odd-A nuclei have revealed various degrees of signature dependence. In particular, large signature dependence of $B(M1)$ values has been observed for several nuclei and they were interpreted as the rotational perturbation effect.[5-9] Those works demonstrated that the information on transition probabilities plays a crucial role in understanding the rotational perturbation of the nuclear system. Moreover, the theoretical works[5-9] suggested that the $B(E2;I\rightarrow I-1)$ values are closely related to deviation of nuclear shape from axial symmetry (including static and dynamic γ deformations) and are important in studying the nuclear shape evolution in high-spin states. In this connection, reliable data are needed especially on $\Delta I=1$ $M1$ and $E2$ transitions.

Here we have studied the ground-state rotational band of ^{161}Dy which is based on the $i_{13/2}$ neutron single-particle state. The level structure of the ground-state rotational band is well established up to high-spin states; we performed a multiple Coulomb excitation experiment to deduce transition probabilities. We have measured γ-ray branchings, $E2/M1$ mixing ratios and nuclear lifetimes, and determined the absolute intraband transition probabilities up to the $\frac{25}{2}^+$ state. The experimental transition probabilities are compared with a microscopic model calculation based on the angular momentum projection method.[10]

The levels of ^{161}Dy have been investigated so far through $(\alpha,3n\gamma)$ (Ref. 11), (n,γ) (Ref. 12), (d,t) (Refs. 12, 13, and 14), and Coulomb excitation with light ions (Refs. 15 and 16). From these works the ground band has been known up to $I=\frac{33}{2}$ (Ref. 17). The low-lying levels of ^{161}Dy were studied in the β^- decay of ^{161}Tb (Ref. 18) and in the electron-capture decay of ^{161}Ho (Refs. 19 and 20). Lifetimes of the ground-band members were deduced only up to the second excited state $\frac{9}{2}^+$ from the Coulomb-excitation experiments (Refs. 15 and 16).

II. EXPERIMENTAL PROCEDURES

First, a self-supporting metallic target of ^{161}Dy (90.4% enriched and about 30 mg/cm^2 thick) was bombarded with a beam of 250-MeV ^{58}Ni from the tandem accelerator at Japan Atomic Energy Research Institute. The target nucleus ^{161}Dy was multiply Coulomb-excited with the beam, which was stopped in the target.

Angular distributions of γ rays were measured with a Compton-suppression spectrometer at seven angles between 0° and 90° to the beam direction. The distance between the target and the spectrometer was 10 cm.

In γ-γ coincidence measurements, three conventional germanium detectors were placed at 0°, 90°, and $-90°$ to the beam. The distance between the target and the detectors was about 7 cm. Those angles were chosen so as to obtain angular correlation information from the expression

$$R=\frac{W(0°,90°)+W(0°,-90°)}{W(90°,0°)+W(-90°,0°)},$$

where the two angles are for the first and second transitions of a γ-ray cascade; the angular correlations, $W(0°,-90°)$ and $W(-90°,0°)$ are equivalent to $W(0°,90°)$ and $W(90°,0°)$, respectively. This is referred to as directional correlation from oriented nuclei (DCO). The data acquisition was controlled by a PDP-11 com-

puter and all events were recorded on magnetic tapes for later analysis.

Lifetime measurements were made by the Doppler-shift recoil-distance method using the 250-MeV ^{58}Ni beam. In this case, the target thickness was 1.3 mg/cm^2. Back-scattered projectiles were measured with a plastic annular scintillator which subtended an angle range of $\theta_{lab}=150°\sim175°$ to the beam direction. Gamma-ray spectra in coincidence with the back-scattered projectiles were measured with a Compton-suppression spectrometer placed at 0° to the beam. The distance between the target and the spectrometer was 13 cm. The average value of the recoil velocity that was determined from the positions of shifted and unshifted γ-ray peaks was 11.4 ± 0.6 μm/psec, which corresponds to $(0.038\pm0.002)c$. The coincidence spectra were measured for seven recoil distances ranging from 50 μm to 1.3 mm. The electric pulse height, which reflects capacitance between the target and stopper, was monitored during the measurements.

III. DATA ANALYSES AND RESULTS

A Compton-suppressed single γ-ray spectrum is shown in Fig. 1. Levels up to $\frac{33}{2}^+$ are confirmed in the coincidence spectra. The angular distributions were fitted with Legendre polynomials

$$W(\theta)=A_0[1+A_2Q_2P_2(\cos\theta)+A_4Q_4P_4(\cos\theta)] .$$

Q_2 and Q_4 are the geometrical attenuation factors, and P_2 and P_4 are the Legendre polynomials. For the detector configuration used, Q_2 and Q_4 were estimated for each γ-ray energy from Ref. 21. The derived coefficients A_2 and A_4 are presented in Table I for the stretched $E2$ and mixed $M1+E2$ transitions. The γ-ray branching between the $\Delta I=1$ and $\Delta I=2$ transitions depopulating a level was obtained from a spectrum gated by a transition just above the level; the effect of angular correlation was taken into account. The γ-ray branchings are presented in Table I in the form of relative intensities.

The experimental A_2 values of the $\Delta I=2$ transitions give the degree of nuclear alignment for the decaying states because these transitions are pure $E2$. We evaluated the degree of alignment for each state, i.e., alignment attenuation factors, α_2 and α_4. These attenuation factors are also presented in Table I.

In order to extract $E2/M1$ mixing ratios for the $\Delta I=1$ transitions, we have analyzed the γ-ray angular distribution and the γ-γ angular correlation data. The $\Delta I=1$ transitions from the states of $\frac{11}{2}^+$, $\frac{13}{2}^+$, $\frac{15}{2}^+$, $\frac{17}{2}^+$, $\frac{21}{2}^+$, and $\frac{25}{2}^+$ have so close energies to others that their angular distribution analyses were not possible. For these transitions, however, the analyses of γ-γ angular correlation were possible because the intruder γ-ray

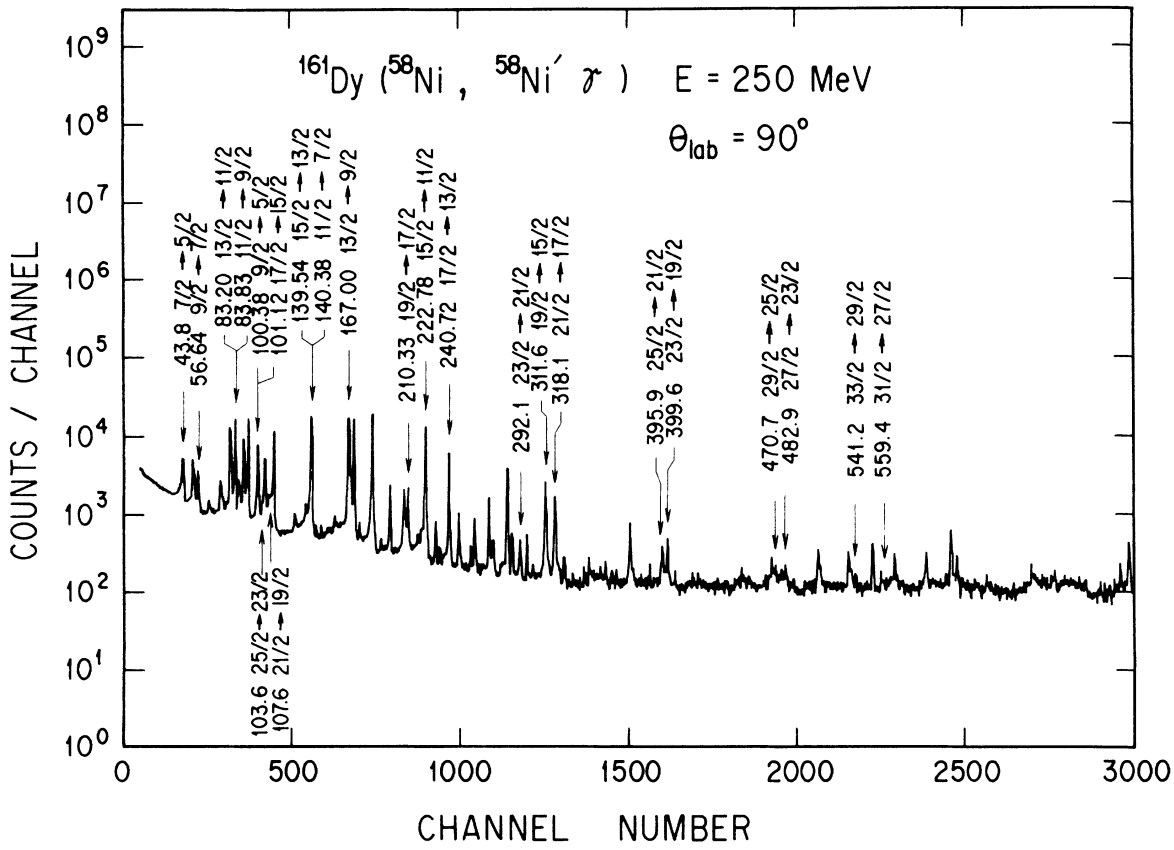

FIG. 1. A Compton-suppressed singles γ-ray spectrum measured at 0° to the beam. Energies are from Ref. 11.

TABLE I. Summary of γ transitions in the ground-state rotational band of ^{161}Dy. E_γ is γ-ray energy given in Ref. 11. I_γ denotes the relative γ-ray intensity normalized to the stronger transition depopulating the state concerned: It was corrected for angular distributions. A_2 and A_4 are angular distribution coefficients. α_2 and α_4 are alignment attenuation factors determined from the stretched $E2$ transitions; α_4 is estimated from α_2 by assuming Gaussian distributions of nuclear alignment (Ref. 22). Figures in parentheses denote uncertainties.

J^π	E_γ (keV)	I_γ	A_2	A_4	α_2	α_4
$\frac{9}{2}^+$	56.64(30)	100				
	100.64(10)	29(4)				
$\frac{11}{2}^+$	83.83(30)	100				
	140.38(30)	74(10)				
$\frac{13}{2}^+$	83.2(3)	75(10)				
	167.0(3)	100	+0.127(8)	+0.008(11)	0.289(18)	0.04
$\frac{15}{2}^+$	139.5(3)	78(11)				
	222.8(3)	100	+0.215(8)	−0.032(5)	0.502(19)	0.14
$\frac{17}{2}^+$	101.1(3)	21.4(8)				
	240.7(3)	100	+0.238(10)	−0.035(8)	0.567(24)	0.18
$\frac{19}{2}^+$	210.3(3)	25.8(14)	−0.58(10)	+0.06(10)		
	311.6(3)	100	+0.259(8)	−0.079(10)	0.626(19)	0.22
$\frac{21}{2}^+$	107.6(3)	6.1(14)				
	318.1(3)	100	+0.283(14)	−0.006(20)	0.69(4)	0.31
$\frac{23}{2}^+$	292.1(3)	23(5)	−0.40(6)	+0.07(8)		
	399.6(3)	100	+0.40(14)	−0.04(4)	0.76[a]	0.40
$\frac{25}{2}^+$	103.6(3)	1.7(2)[b]				
	395.9(3)	100	+0.55(20)	−0.05(18)	0.82[a]	0.51
$\frac{27}{2}^+$	380.0(3)	42(4)[b]				
	482.9(3)	100	+0.60(35)	−0.09(9)	0.87[a]	0.57

[a]Estimated by a Coulomb-excitation calculation code (Ref. 23), because the experimental A_2 values have large uncertainties.
[b]From Ref. 11. The uncertainty of 10% was assumed.

peaks could be eliminated by gating on appropriate transitions. We calculated first the DCO ratios for the spin sequence of $I+2(E2)I(E2)I-2$ to check validity of the DCO analyses. Corrections for detection efficiencies of the germanium detectors were made in obtaining the DCO ratios. The ratios are shown in Table II and are

TABLE II. DCO ratios (R) for the spin sequence of $I+2\rightarrow I\rightarrow I-2$.

Spin sequence	R
$\frac{13}{2}\rightarrow\frac{9}{2}\rightarrow\frac{5}{2}$	1.29(25)
$\frac{15}{2}\rightarrow\frac{11}{2}\rightarrow\frac{7}{2}$	0.99(5)
$\frac{17}{2}\rightarrow\frac{13}{2}\rightarrow\frac{9}{2}$	1.03(5)
$\frac{19}{2}\rightarrow\frac{15}{2}\rightarrow\frac{11}{2}$	1.04(9)
$\frac{21}{2}\rightarrow\frac{17}{2}\rightarrow\frac{13}{2}$	0.97(5)
$\frac{23}{2}\rightarrow\frac{19}{2}\rightarrow\frac{15}{2}$	1.02(5)
$\frac{25}{2}\rightarrow\frac{21}{2}\rightarrow\frac{17}{2}$	0.96(9)
$\frac{27}{2}\rightarrow\frac{23}{2}\rightarrow\frac{19}{2}$	0.91(5)
$\frac{29}{2}\rightarrow\frac{25}{2}\rightarrow\frac{21}{2}$	1.18(10)

TABLE III. Summary of $E2/M1$ mixing ratios δ for the $\Delta I=1$ transitions. They are obtained from the γ-γ angular correlation data unless otherwise noted.

$I\rightarrow I-1$	$R(A)$	$R(B)$	δ
$\frac{7}{2}\rightarrow\frac{5}{2}$			0.2[a]
$\frac{9}{2}\rightarrow\frac{7}{2}$			0.22[a]
$\frac{11}{2}\rightarrow\frac{9}{2}$		0.46(3)	−0.25(7)
$\frac{13}{2}\rightarrow\frac{11}{2}$		0.48(2)	−0.14(2)
$\frac{15}{2}\rightarrow\frac{13}{2}$	2.26(5)		−0.27(3)
$\frac{17}{2}\rightarrow\frac{15}{2}$		0.51(2)	−0.05(2)
$\frac{19}{2}\rightarrow\frac{17}{2}$	2.86(18)	0.34(3)	−0.27(4)[b]
$\frac{21}{2}\rightarrow\frac{19}{2}$	1.96(8)	0.47(5)	−0.05(2)[c]
$\frac{23}{2}\rightarrow\frac{21}{2}$	4.3(6)		−0.23(7)[b]
$\frac{25}{2}\rightarrow\frac{23}{2}$	2.30(35)		−0.03(3)

[a]Absolute value derived from Ref. 17.
[b]Obtained from a combined analysis of the γ-ray angular distribution and the γ-γ angular correlation data.
[c]Obtained from a combined analysis of the γ-γ angular correlation data [$R(A)$ and $R(B)$].

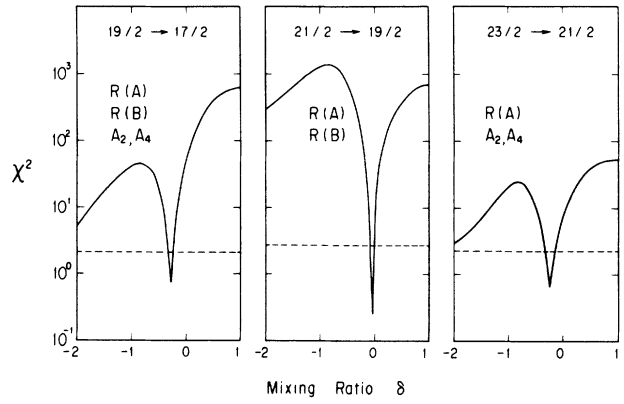

FIG. 2. Mixing ratio analyses for the $\frac{19}{2} \rightarrow \frac{17}{2}$, $\frac{21}{2} \rightarrow \frac{19}{2}$, and $\frac{23}{2} \rightarrow \frac{21}{2}$ transitions, in which more than two of the quantities [$R(A)$, $R(B)$, or $A_2(A_4)$] are available. The reduced χ^2 due to those quantities is plotted as a function of δ in each of the figures. The uncertainty was estimated for a 90% confidence level shown with a dashed line in the figures.

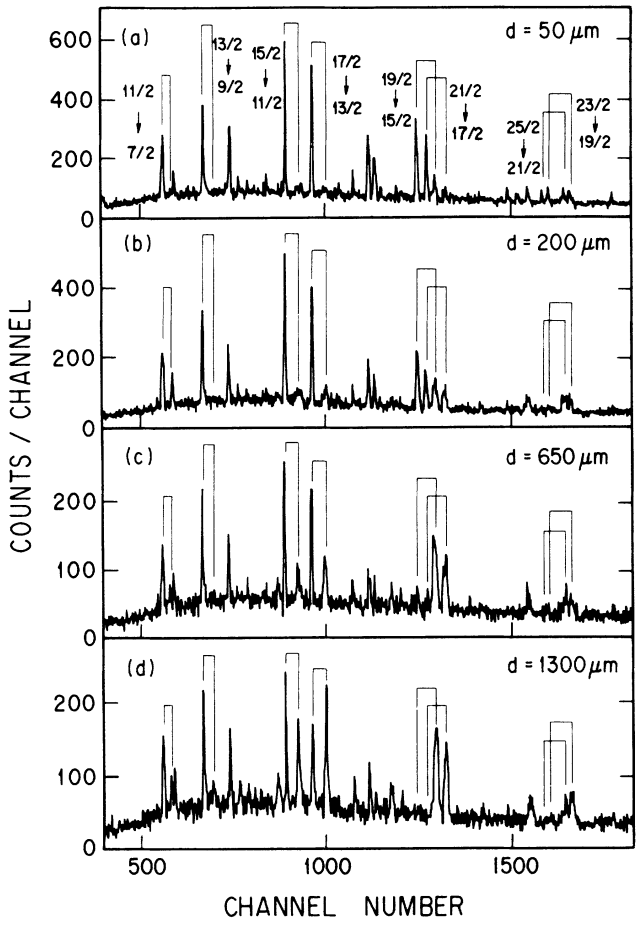

FIG. 3. Illustrative particle-gated γ-ray spectra of ^{161}Dy covering the 200–700 keV region for four of the ten distances measured.

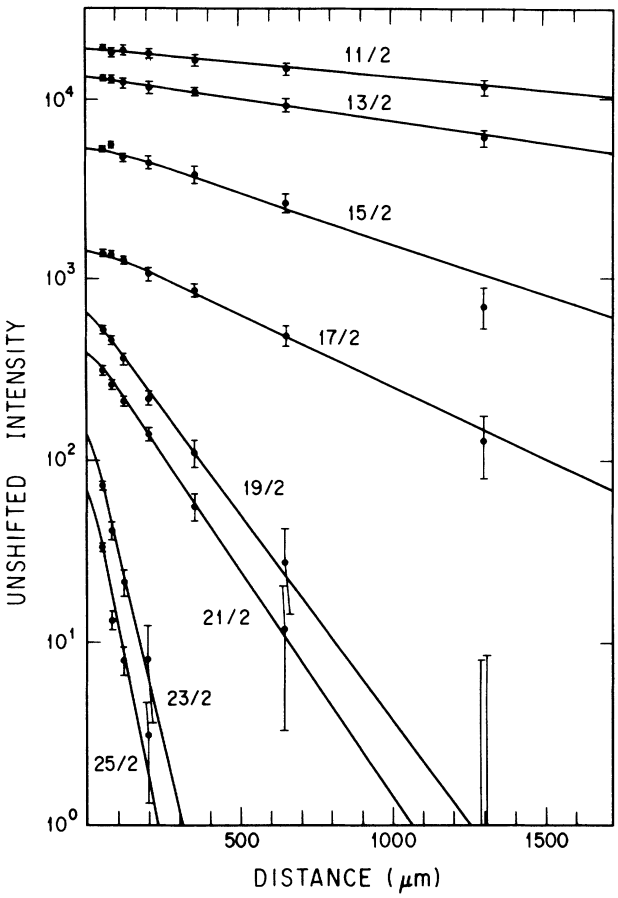

FIG. 4. Decay curves for the ground-band members of ^{161}Dy.

very close to unity within the experimental uncertainties. This shows that the present DCO measurement is reliable because the theoretical ratios for the spin sequence of $I+2(E2)I(E2)I-2$ are equal to unity in the present geometry.[24]

The DCO data for the $\Delta I=1$ transitions were analyzed in the method described in Refs. 3 and 24. Two types of DCO analyses have been made: One is for the spin sequence of $I(M1+E2)I-1(E2)I-3$ and the other for $I+2(E2)I(M1+E2)I-1$, where $M1+E2$ indicates the transition of interest. The former type of the DCO ratios is denoted by $R(A)$ and the latter by $R(B)$ in Table III. The alignment attenuation factors α_2 and α_4 determined by the angular distributions for the stretched $E2$ transitions (see Table I) were used in this analysis. For the $\frac{19}{2} \rightarrow \frac{17}{2}$, $\frac{21}{2} \rightarrow \frac{19}{2}$, and $\frac{23}{2} \rightarrow \frac{21}{2}$ transitions, for which more than two of the quantities [$R(A)$, $R(B)$, or $A_2(A_4)$] are available, combined analyses have been made as shown in Fig. 2. In other cases, the mixing ratio δ is determined directly from the DCO ratio. The uncertainty was estimated by taking 1.6 times the standard deviation (90% confidence). The derived mixing ratios together with the DCO ratios are summarized in Table III.

The Doppler-shift recoil-distance method was used to determine nuclear lifetimes. In Fig. 3 we show particle-gated spectra taken at four of the target-stopper separations. Decay curves derived from the spectra were ana-

TABLE IV. Summary of lifetimes and reduced transition probabilities.

I	τ (ps)	$B(E2;I\to I-2)$ (e^2b^2)	$B(M1;I\to I-1)$ (μ_N^2)	$B(E2;I\to I-1)$ (e^2b^2)
$\frac{7}{2}$	1130(90)[a]		0.061(18)[a]	1.82(5)[b]
$\frac{9}{2}$	300(3)[b]	0.48(2)[a]	0.063(19)[a]	1.36(41)[a]
$\frac{11}{2}$	225(20)	0.78(12)	0.064(19)	0.82(45)
$\frac{13}{2}$	144(13)	0.82(11)	0.094(18)	0.38(13)
$\frac{15}{2}$	60(7)	0.93(12)	0.095(18)	0.51(14)
$\frac{17}{2}$	47(5)	1.16(12)	0.134(14)	0.047(38)
$\frac{19}{2}$	16.2(18)	1.25(14)	0.066(8)	0.16(5)
$\frac{21}{2}$	14.9(14)	1.36(14)	0.149(37)	0.047(39)
$\frac{23}{2}$	5.1(6)	1.22(13)	0.076(19)	0.068(43)
$\frac{25}{2}$	4.3(8)	1.80(35)	0.185(40)	0.02(5)

[a]From Ref. 17.
[b]From Ref. 15.

lyzed by a computer program LIFETIME.[25] The Coulomb excitation process does not cause any serious side-feeding contribution to the decay curves which often brings considerable uncertainty of the final result in compound nuclear residues. This feature enables the lifetimes of excited states to be determined accurately.

The results of the recoil-distance analysis are shown in Fig. 4. The lifetimes obtained for the states from $\frac{11}{2}^+$ to $\frac{25}{2}^+$ are summarized in Table IV.

IV. MICROSCOPIC MODEL CALCULATION

We carried out a microscopic calculation using the Nilsson plus BCS (deformed quasiparticle) representation. Since we are interested in the transition probabilities, we need to construct microscopic wave functions with definite angular momenta. For this purpose, we employed the angular momentum projection (AMP) method.[10] The AMP method has been successfully applied to the description of the energy spectra of odd-mass rare-earth nuclei.[10] Since the details of the calculation method are given in Ref. 10, we present here the outline of the method only. The Hamiltonian employed is the sum of the spherical single-particle Hamiltonian, the monopole pairing force, the QQ force and the quadrupole pairing force:

$$\hat{\mathcal{H}}=\hat{h}-G_M\hat{P}^\dagger\hat{P}-\tfrac{1}{2}\chi\sum_\mu\hat{Q}_\mu^\dagger\hat{Q}_\mu-G_Q\sum_\mu\hat{P}_\mu^\dagger\hat{P}_\mu \ .$$

For the monopole force strength we take the values $G_M=[20.124\pm13.131(N-Z)/A]$ MeV for neutrons $(-)$ and protons $(+)$. The quadrupole-force strength χ is determined so that the Hartree-Bogoliubov approximation for the pairing plus QQ part of the Hamiltonian is equal to the Nilsson plus pairing-force model with the axially symmetric quadrupole deformation $\epsilon_2=0.251$. The strength of the quadrupole pairing force G_Q is assumed to be proportional to the monopole pairing force strength as $G_Q=0.2G_M$. Note that the quadrupole pairing force of this strength is needed to obtain reasonable values of the moment of inertia for the rare-earth nuclei and to properly attenuate the Coriolis coupling in odd-mass nuclei.[10] In the present calculation three shells are taken into account for each nucleon, i.e., $N=4,5,6$ for neutrons and $N=3,4,5$ for protons.

To treat the effects of rotation fully quantum mechanically, we diagonalize the Hamiltonian within the space spanned by a set of angular momentum projected one-quasiparticle states $\hat{P}^I_{MKi}a_i^\dagger\,|\,0\rangle$, where $|\,0\rangle$ is the axially-symmetric Nilsson plus BCS vacuum. The resulting equation of motion is

$$\hat{\mathcal{H}}\,|\,\Psi_{nI}\rangle=E_{nI}\,|\,\Psi_{nI}\rangle \ ,$$

where

$$|\,\Psi_{nI}\rangle=\sum_i f_i\hat{P}^I_{MK_i}a_i^\dagger\,|\,0\rangle \ .$$

Since we use the angular momentum projected basis, we can easily evaluate the matrix elements of an observable $\hat{0}^\lambda_\mu$, $\langle\Psi_{nI}\,|\,\hat{0}^\lambda_\mu\,|\,\Psi_{n'I'}\rangle$, using the following formula:

$$\langle 0\,|\,a_i\hat{P}^I_{K_iM}\hat{0}^\lambda_\mu\hat{P}^{I'}_{M'K_i'}a_{i'}^\dagger\,|\,0\rangle$$
$$=\langle I'\lambda M'\mu\,|\,IM\rangle\times\sum_\nu\langle I'\lambda K_i-\nu\nu\,|\,IK_i\rangle\langle 0\,|\,a_i\hat{0}^\lambda_\nu\hat{P}^{I'}_{K_i-\nu K_i'}a_{i'}^\dagger\,|\,0\rangle \ .$$

In Ref. 10 a detailed explanation is given for the evaluation of the matrix element $\langle 0\,|\,a_i\hat{0}^\lambda_\nu\hat{P}^{I'}_{K_i-\nu K_i'}a_{i'}^\dagger\,|\,0\rangle$.

V. DISCUSSION

From the lifetimes, the γ-ray branchings and the $E2/M1$ mixing ratios, the reduced transition probabilities of $B(E2;I\to I-2)$, $B(M1;I\to I-1)$, and $B(E2;I\to I-1)$ have been derived as presented in Table IV. The $B(E2;I\to I-2)$ and $B(M1;I\to I-1)$ are also shown in Figs. 5 and 6, and are compared with the present AMP calculations. As shown in Fig. 5, the calcu-

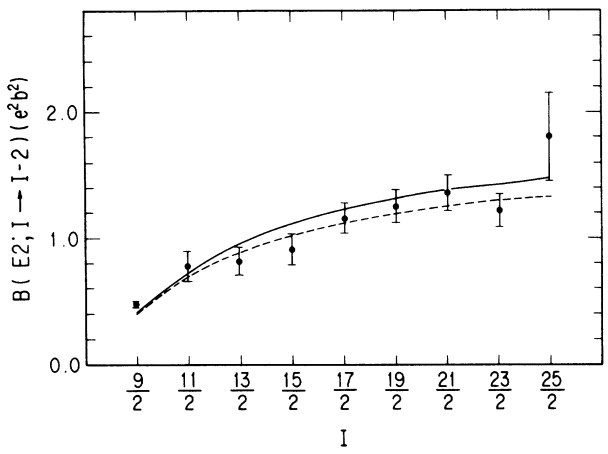

FIG. 5. The $B(E2;I\rightarrow I-2)$ values for the ground-state rotational band of ^{161}Dy. The experimental value for $I=\frac{9}{2}$ is from Ref. 17, and others are the present data. The dashed line denotes a strong coupling estimate (Ref. 26): $B(E2;I\rightarrow I-2)=(5/16\pi)Q_0^2\langle I2K0\,|\,I-2K\rangle^2$, where $Q_0=6.5b$ is adopted to fit the experimental values. The solid line denotes the present AMP calculation.

lation of the $B(E2;I\rightarrow I-2)$ shows no significant signature dependence and has turned out to be very close to the prediction of the Bohr-Mottelson strong coupling model.[26] Both calculations are in good agreement with the experimental $B(E2;I\rightarrow I-2)$ values. This suggests that the $B(E2;I\rightarrow I-2)$ values are determined essentially by the deformed core.

In Fig. 6, the experimental $B(M1;I\rightarrow I-1)$ values show an apparent oscillation above $I=\frac{13}{2}$. The $B(M1;I_i=j+2n\rightarrow I_f=j+2n-1)$ values, where j is the single-particle angular momentum and n is an integer, become larger than the $B(M1;I_i=j+2n+1\rightarrow I_f=j+2n)$. The AMP calculation is in good agreement with the experimentally observed signature dependence of the $B(M1)$; this supports an interpretation of this phenomenon as the perturbation effect of rotation.[5–9]

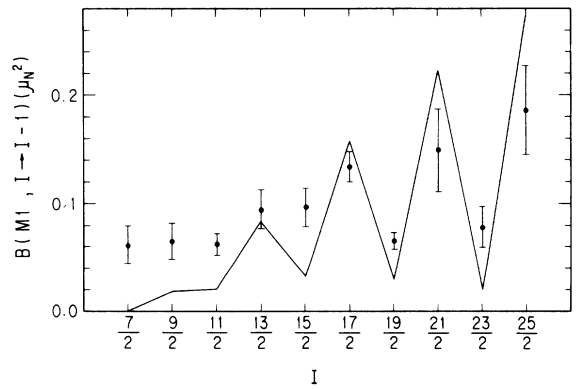

FIG. 6. The $B(M1;I\rightarrow I-1)$ values for the ground-state rotational band of ^{161}Dy. The experimental values for $I=\frac{7}{2}$ and $I=\frac{9}{2}$ are from Ref. 17, and others the present data. The solid line denotes the present AMP calculation.

We define the $\Delta I=1$ and $\Delta I=2$ transition quadrupole moments by

$$Q(\Delta I)=\left[\frac{16\pi}{5}B(E2;I\rightarrow I-\Delta I)/\langle I2K0\,|\,I-\Delta IK\rangle^2\right]^{1/2},$$

where $\langle I2K0\,|\,I-\Delta IK\rangle$ is a Clebsch-Gordan coefficient. In order to compare the $Q(\Delta I=1)$ with the $Q(\Delta I=2)$, the ratio $Q(\Delta I=1)/Q(\Delta I=2)$ is plotted as a function of spin in Fig. 7. Since there is no significant signature dependence of the experimental $B(E2;I\rightarrow I-2)$ values (see Fig. 5), the major features in Fig. 7 must be ascribed to the $Q(\Delta I=1)$. As shown in Fig. 7, the ratio is always smaller than unity and decreases considerably as the spin value increases. The ratio appears to have a weak signature dependence with the phase opposite to that for the $B(M1)$. The present AMP calculation for axially-symmetric nuclear shape (a solid line in Fig. 7) reproduces approximately the ratio $Q(\Delta I=1)/Q(\Delta I=2)$ for lower spin states, but hardly reproduces the marked reduction of the ratio for the higher spin ($I\geq\frac{17}{2}$) states. One might think that the introduction of the γ degrees of freedom explains this reduction of the ratio.[5] According to the calculation for ^{161}Dy by Matsuzaki *et al.*,[27] which includes both static and dynamic γ deformations, the effect due to the γ deformations is not strong enough to reproduce the reduction of the ratio.

It is interesting to compare our result with that for the rotational band built on the $h_{11/2}$ orbital in ^{157}Ho (Ref. 2). There is a striking difference between them: The $Q(\Delta I=1)/Q(\Delta I=2)$ for ^{157}Ho is mostly greater than unity in the region of $I=\frac{13}{2}$ to $\frac{33}{2}$; and the ratio oscillates with a large amplitude $[1\leq Q(\Delta I=1)/Q(\Delta I=2)\leq 2]$. The phase of the signature dependence coincides with that for the $B(M1)$ in ^{157}Ho.

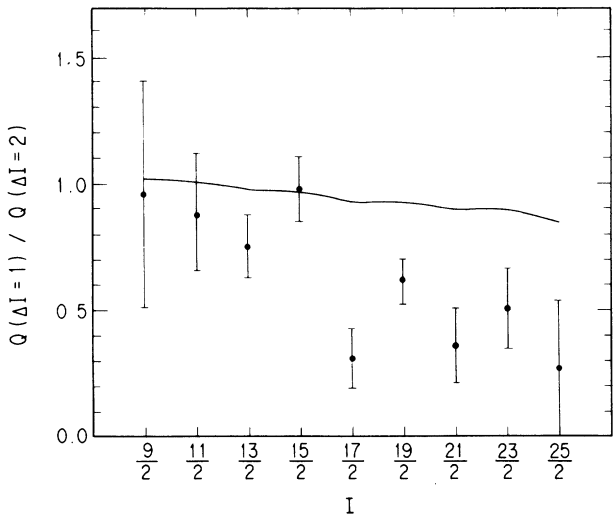

FIG. 7. The ratio of $\Delta I=1$ transition quadrupole moments to that of $\Delta I=2$. The solid line denotes the present AMP calculation.

VI. SUMMARY

The experimental $B(E2;I\rightarrow I-2)$ values for the ground-state rotational band of ^{161}Dy show almost no signature dependence. They were reproduced well by the present AMP calculation which assumes axial symmetry of the nuclear shape.

On the other hand, a significant signature dependence was observed for the $B(M1;I\rightarrow I-1)$ values. The experimental values were well reproduced by the present AMP calculation, where the effect of rotation was treated both microscopically and quantum mechanically. This supports the interpretation that the signature dependence of the $B(M1)$ values is due to the perturbation effect of rotation.[5–9]

The $Q(\Delta I=1)$ moments deduced from the $B(E2;I\rightarrow I-1)$ values for the high spin ($I\geq\frac{17}{2}$) states are considerably smaller than those for the $I\rightarrow I-2$ transitions; the $Q(\Delta I=1)$ moments seem to have a weak signature dependence. At present, the small $Q(\Delta I=1)$ moments and their signature dependence are hardly explained by current models, e.g., the AMP method and the models with the γ degrees of freedom.[5–8,27] Further refinement of the theoretical models is needed to solve this problem for the $B(E2;I\rightarrow I-1)$.

ACKNOWLEDGMENTS

We wish to thank the crew of the JAERI tandem accelerator for providing the needed heavy-ion beams. We are grateful to Dr. A. Ikeda and Dr. M. Matsuzaki for valuable discussions. We would also like to thank Dr. N. Shikazono, Dr. M. Ishii, and Dr. H. Kamitsubo for their support of this study. This study has been carried out as a joint research program between JAERI and RIKEN.

[1] J. Kownacki, J. D. Garrett, J. J. Gaardhøje, G. B. Hagemann, B. Herskind, S. Jónsson, N. Roy, H. Ryde, and W. Walus, Nucl. Phys. **A394**, 269 (1983).

[2] G. B. Hagemann, J. D. Garrett, B. Herskind, J. Kownacki, B. M. Nyakó, P. L. Nolan, J. F. Sharpey-Schafer, and P. O. Tjøm, Nucl. Phys. **A424**, 365 (1984).

[3] M. Ohshima, E. Minehara, M. Ishii, T. Inamura, and A. Hashizume, Nucl. Phys. **A436**, 518 (1985).

[4] S. Jónsson, J. Lyttkens, L. Carlén, N. Roy, H. Ryde, W. Waluś, J. Kownacki, G. B. Hagemann, B. Herskind, J. D. Garrett, and P. O. Tjøm, Nucl. Phys. **A422**, 397 (1984).

[5] I. Hamamoto, Phys. Lett. **106B**, 281 (1981); Nucl. Phys. **A421**, 109c (1984); I. Hamamoto and B. R. Mottelson, Phys. Lett. **132B**, 7 (1983).

[6] A. Ikeda, Nucl. Phys. **A439**, 317 (1985).

[7] M. Matsuzaki, Y. R. Shimizu, and K. Matsuyanagi, Prog. Theor. Phys. **77**, 1302 (1987).

[8] N. Onishi, I. Hamamoto, S. Åberg, and A. Ikeda, Nucl. Phys. **A452**, 71 (1986).

[9] Y. S. Chen, P. B. Semmes, and G. A. Leander, Phys. Rev. C **34**, 1935 (1986).

[10] K. Hara and S. Iwasaki, Nucl. Phys. **A332**, 61 (1979); *ibid.* **A348**, 200 (1980); *ibid.* **A430**, 175 (1984).

[11] S. A. Hjorth, A. Johnson, and G. Ehrling, Nucl. Phys. **A184**, 113 (1972).

[12] M. J. Bennett and R. K. Sheline, Phys. Rev. C **15**, 146 (1977).

[13] T. Grotdal, K. Nybo, and B. Elbek, Mat. Fys. Medd. Dan. Vid. Selsk. **37**, No. 12 (1970).

[14] J. C. Peng, J. V. Maher, G. H. Wedberg, and C. M. Cheng, Phys. Rev. C **13**, 1451 (1976).

[15] P. F. Brown, C. Baktash, J. O'Brien, and J. X. Saladin, Phys. Rev. C **18**, 666 (1978).

[16] D. Ashery, N. Bahcall, G. Goldring, A. Sprinzak, and Y. Wolfson, Nucl. Phys. **A101**, 51 (1967).

[17] R. G. Helmer, Nucl. Data Sheets **43**, 1 (1984).

[18] K. G. Prasad and H. L. Nielsen, Phys. Scr. **9**, 208 (1974).

[19] K. Ya. Gromov, T. A. Islamov, N. A. Lebedev, T. M. Muminov, U. S. Salikhbaev, A. A. Tangabaev, and E. G. Tsoi, Program and Thesis, Proceedings of the 31st Annual Conference on Nuclear Spectroscopy and Structure of Atomic Nuclei, Samarkand (1981), p. 123.

[20] A. A. Abdurazakov, K. Y. Gromov, V. V. Kuznetsov, Ma Ho Ik, G. Muziol, F. Molnar, A. Molnar, F. Mukhtasimov, and S. J. Han, Yad. Fiz. **1**, 951 (1965).

[21] D. C. Camp and A. L. Van Lehn, Nucl. Instrum. Methods **76**, 192 (1969).

[22] H. Morinaga and T. Yamazaki, *In-Beam Gamma-Ray Spectroscopy* (North-Holland, Amsterdam, 1976).

[23] A. Winther and J. de Boer, in *Coulomb Excitation*, edited by K. Alder and A. Winther (Academic, New York, 1966), p. 303.

[24] K. S. Krane, R. M. Steffen, and R. M. Wheeler, Nucl. Data Tables **11**, 351 (1973).

[25] J. C. Wells, M. P. Fewell, and N. R. Johnson, Oak Ridge National Laboratory Report ORNL/TM-9105, 1985.

[26] A. Bohr and Mottelson, *Nuclear Structure* (Benjamin, New York, 1975), Vol. 2.

[27] M. Matsuzaki, Y. R. Shimizu, and K. Matsuyanagi (submitted to Prog. Theor. Phys).